Molecular Vision 2025; 31:127-141 <http://www.molvis.org/molvis/v31/127>
Received 15 February 2024 | Accepted 27 March 2025 | Published 29 March 2025

Subretinal delivery of AAV5-mediated human *Pde6b* gene ameliorates the disease phenotype in a rat model of retinitis pigmentosa

Hee Jong Kim,[1,2] Ji Hoon Kwak,[3,4] Jun Sub Choi,[1,2] Jin Kim,[1,2] Seo Yun Moon,[1,2] Steven Hyun Seung Lee,[1,2] Heuiran Lee,[5,6] Keerang Park,[1,2] Joo Yong Lee,[3,4] So-Yoon Won[1,2]

(The first two authors contributed equally to this work.)

[1]Institute of New Drug Development Research, CdmoGen Co., Ltd., Seoul, Republic of Korea; [2]CdmoGen Co., Ltd., Cheongju, Republic of Korea; [3]Department of Ophthalmology, Asan Medical Center, University of Ulsan, College of Medicine, Republic of Korea; [4]Bio-Medical Institute of Technology, University of Ulsan, College of Medicine, Republic of Korea; [5]Department of Microbiology, Asan Medical Center, University of Ulsan College of Medicine, Seoul; [6]Bio-Medical Institute of Technology, College of Medicine, University of Ulsan, Seoul, Republic of Korea

Purpose: A genetic disorder that affects the beta subunit of cyclic guanosine monophosphate-phosphodiesterase type 6 (PDE6B) in humans leads to autosomal recessive retinitis pigmentosa (RP). This condition causes severe vision loss in early life due to fast deterioration of photoreceptors. This study evaluated the therapeutic potential of subretinal delivery of the adeno-associated virus (AAV)5-mediated human *Pde6b* gene in an RP rat model caused by *Pde6b* gene knockout (KO).

Methods: We compared the transduction efficiency and tropism of different AAV serotypes (2, 5 and 8) in *Pde6b* KO rats and found that AAV5 had the highest and most specific expression in photoreceptors. We injected AAV5-*Pde6b* into the subretinal space of *Pde6b* KO rats on postnatal day 21. We assessed the protective effects six weeks postinjection by measuring PDE6B protein expression, photoreceptor structure, retinal morphology and thickness, retinal pigment epithelium integrity and visual function.

Results: AAV5-*Pde6b* treatment ameliorated the disease phenotype in *Pde6b* KO rats by restoring PDE6B protein expression, preserving photoreceptor structure, improving retinal morphology and thickness, and maintaining retinal pigment epithelium integrity. Functional analysis of vision by scotopic electroretinogram (ERG) and optokinetic nystagmus revealed that AAV5-*Pde6b* treatment significantly improved the visual function of *Pde6b* gene KO rats compared with AAV5-*GFP*-injected *Pde6b* KO rats.

Conclusions: Our results demonstrate that AAV5-*Pde6b* may be a potential therapeutic gene candidate for RP caused by *Pde6b* mutations.

Retinitis pigmentosa (RP) is a hereditary disease that affects the retina, which is the light-sensitive tissue at the back of the eye [1,2]. RP causes the gradual loss of photoreceptor cells responsible for converting light into electrical signals [1,3]. As a result, people with RP experience progressive vision impairment, often leading to legal blindness [1,3]. RP affects about one in every 4,000 people worldwide and is one of the most common causes of inherited blindness [4]. Many genetic factors can cause RP [5], and more than 80 genes linked to nonsyndromic RP, meaning RP that occurs without any other symptoms or conditions, have been identified so far [6].

Correspondence to: So-Yoon Won, CdmoGen, Institute of New Drug Development Research #1023, A Dong,201, Songpa-daero, Seoul, Seoul 05855, Republic of South Korea; Phone: 82-2-881-5419; FAX: 82432362277; email: sywon@cdmogen.com

One of these genes is *Pde6b*, which encodes the phosphodiesterase 6β (PDE6B) subunit of the PDE6 protein [7]. The PDE6 protein of phosphodiesterase plays a crucial role in the phototransduction process, which is the mechanism by which light is converted into electrical signals in the retina [8,9]. This process begins when photons of light activate Rhodopsin, a photoreceptor protein. Activated Rhodopsin then stimulates the G-protein transducin, activating the enzyme PDE6. PDE6B is a subunit of this enzyme and is essential for its function. Once activated, PDE6 lowers the concentration of cyclic guanosine monophosphate (cGMP) within the cell, leading to closure of cGMP-gated ion channels, resulting in hyperpolarization of the photoreceptor cell and the initiation of a signal to the brain that light has been detected [9,10].

Mutations in *Pde6b* can impair the function of PDE6B, leading to abnormal levels of cGMP and defective

phototransduction. This can cause the rod cells to degenerate and die, reducing night vision and peripheral vision. Over time, this can also affect the cone cells, the photoreceptors that enable color vision and fine details. Mutations in *Pde6b* account for 5%–8% of cases of autosomal recessive RP, meaning that both copies of the gene must be mutated for the disease to occur [11,12].

Gene therapy delivers healthy copies of defective genes to the retina or modifies existing gene expression, and is a promising approach for RP treatment [1]. Several gene therapy trials are underway for different forms of RP targeting specific mutations or pathways involved in the disease. For example, Luxturna is an approved gene therapy product that corrects mutations in the *RPE65* gene, which is responsible for a rare form of RP that affects night vision [13]. A recent study also showed that gene therapy with *Nrf2*, a transcription factor that regulates antioxidant response, was able to reverse retinal pigment epithelium (RPE) degeneration and protect photoreceptors in a mouse model of RP [14,15]. Gene therapy for RP faces several challenges, such as the diversity of genetic causes, delivery methods, safety and efficacy and ethical issues [16,17].

Adeno-associated viruses (AAVs) are widely used as vectors for retinal gene therapy as they can transduce various cell types and have low immunogenicity [5]. However, various AAV serotypes show differences in expression efficiency depending on the route of administration, and the tropism of each serotype is known to vary depending on the target tissue [18,19]. Therefore, choosing the optimal AAV serotype and delivery method is crucial for therapeutic efficacy. Intravitreal and subretinal injections are two standard gene therapy methods for the retina. Intravitreal injections are performed by inserting a needle through the sclera and into the vitreous humor, the gel-like substance that fills the eye [20]. Subretinal injections create a small retinal detachment and inject the gene therapy under the retina [21]. Both methods have advantages and disadvantages, depending on the type and location of retinal disease, the size and volume of the gene therapy vector, and the potential side effects and complications [22].

Although mouse strains harboring *Pde6b* mutant alleles (*rd1* [Pde6brd1] and *rd10* [Pde6brd10]) are considered animal models of RP and are the most widely used models [23,24], rats are considered more suitable models for RP treatment due to their anatomic and physiologic similarities to humans, which may improve the applicability of research findings to human therapies [25,26]. Additionally, their larger size compared with mice minimizes the risk of complications during intricate procedures such as subretinal injections, which are often problematic in animals with smaller eyes [27-31]. We previously developed a stable *Pde6b* knockout (KO) rat model using clustered regulated interspaced short palindromic repeats (CRISPR)-Cpf1 technology, which causes retinal degeneration [32]. In the present study, we evaluated the efficacy of subretinal delivery of the AAV5-mediated human *Pde6b* gene (AAV5-*Pde6b*) in an RP rat model caused by *Pde6b* gene KO. We compared the transduction efficiency and tropism of AAV serotypes 2, 5 and 8 in *Pde6b* KO rats, depending on the route of administration. We also assessed the therapeutic effects of clinical phenotype, PDE6B protein expression, retinal morphology and visual function in AAV5-*Pde6b* treated *Pde6b* KO rats. Here we aimed to show that subretinal injection of AAV5-*Pde6b* improves the disease phenotype in *Pde6b* KO mice and provides proof-of-concept for gene therapy of RP caused by *Pde6b* mutations.

METHODS

Experimental animals: The experiments used 12 six-week-old Sprague-Dawley (SD) rats and 16 three-week-old *Pde6b*-KO rats, which CRISPR-Cpf1 produced in our previous publishments [32]. SD rats were housed two to three per cage with ad libitum access to water and food during a 12-h light/dark cycle. All reasonable efforts were made to minimize animal suffering and to use the minimum number of animals necessary to perform statistically valid analyses. The study was conducted by the Declaration of Helsinki and approved by the Institutional Review Board of Animal Experiments at the Asan Institute for Life Science (University of Ulsan, College of Medicine; protocol code 2022–12–210, 11 August 2022).

AAV vector production: The human phosphodiesterase 6B gene (PDE6B, NM_000283.4) was used to construct a photoreceptor *Pde6b* gene insert. The insert was verified by sequencing and then packaged into AAV5 vectors by co-transfecting 293T cells with three plasmids comprising pAAV-CMV-h*Pde6b* (pAAV-*Pde6b*), pR2C5 and pHelper. The resulting virus, AAV5-*Pde6b*, was purified and frozen (−80 °C) in sterile tubes for later use. All virus vectors used in this study were obtained from CdmoGen Co., Ltd. (Cheongju, Korea).

Delivery of viral vector (intravitreal and subretinal injection): The rats were anesthetized via intraperitoneal injection of a combination of alfaxalone (20 mg/kg, Alfaxan, Jurox Pty Ltd., NSW, Australia) and xylazine (10 mg/kg, Rompun, Elanco Inc., Greenfield, IN). The intravitreal injections were administered using a 33-G Hamilton syringe (Hamilton, Bonaduz, Switzerland) and the procedure was guided by an operating microscope (Zeiss, Oberkochen, Germany). Pupil dilation was achieved using Mydrin-P, consisting of

tropicamide 5 mg/ml and phenylephrine 5 mg/ml (Santen Pharmaceuticals, Osaka, Japan). A sclerotomy was carefully performed approximately 1 mm posterior to the limbus for intravitreal injections using a 33-G Hamilton syringe. This was carried out with due care to avoid causing any damage to the lens. An amount of 5 µl AAV2, -5 or -8-*GFP* (5.02×10^{10} vg/ml) was administered intravitreally. Subretinal injection required a temporal conjunctival peristome, after which subretinal injection was performed using the same needle and the AAV2, -5 or -8-*GFP* dose. The accuracy of each injection was assessed via a fundus camera and in vivo fluorescence imaging, as previously described. To prevent intraocular infection and excessive dehydration during recovery after imaging, the eyes were treated with Tarivid ointment (Ofloxacin 3 mg/g, Santen Pharmaceuticals).

Histologic analysis: For those cases with cryosectioned retinas, the eyes were enucleated and fixed overnight with 4% PFA and underwent gradient dehydration with sucrose. Subsequently, the processed eyes were snap-frozen in optimal cutting temperature compound. The retinas were blocked in phosphate-buffered saline with Tween (PBST; 0.5% Triton X-100 in PBS) and treated overnight with 5% normal goat serum with an anti-PDE6B antibody at 4 °C. Following a wash in 0.5% PBST, the samples were incubated for 4 h at room temperature with species-specific Alexa Fluor-coupled secondary antibodies. 4’,6-diamidino-2-phenylindole (DAPI)/Hoechst dyes were used to identify the nucleus. The samples were washed in 0.5% PBST at least five times and mounted with a mounting medium (Vectashield, Vector Laboratories, Burlingame, CA). A Zeiss LSM 780 confocal microscope (Carl Zeiss, Berlin, Germany) was used to obtain immunofluorescence data. Primary antibodies were diluted in an antibody Diluent (Dako, S3022, Agilent-Dako, Canada). We used the following primary antibodies in this study: anti-*GFP* (sc-8334, 200 mg/ml, Santa Cruz Biotechnology, Dallas, TX; IF: 1:100), anti-PDE6B (GTX33395, Gene Tex, Irvine, CA; IF: 1:100), anti-Rhodopsin (ab221664, Abcam, Cambridge, UK, IF: 1:100) and anti-phalloidin (P1951, 300 units, Millipore-Sigma, Burlington, MA; IF: 1:1000). Retinal tissue sections were incubated with Alexa 488- or Alexa 594-conjugated secondary antibodies for fluorescence microscopy and the nuclei were counterstained using DAPI (Thermo Fisher Scientific, Waltham, MA). The retinal tissue sections were stained with hematoxylin and eosin (H&E) and photographed under a microscope (Olympus CX41; Olympus America, Center Valley, PA) at 320× and 340× magnification.

Fundus examination and imaging: Topical anesthesia was achieved using proparacaine hydroxychloride (Alcaine; Alcon, Fort Worth, TX). The eyes were dilated with 1% tropicamide and 2.5% phenylephrine drops (Mydrin-P; Santen Pharmaceuticals) and lubricated with methylcellulose. Fundus photographs were taken using the Micron IV (Phoenix Research Laboratories, Pleasanton, CA), with a wavelength range between 450 and 650 nm; acquired images were stored in Micron IV software (StreamPix; NorPix, Inc., Montreal, QC, Canada).

Optical coherence tomography: Sectional retina images were acquired using image-guided optical coherence tomography (OCT; OCT2; Phoenix Research Laboratories, OR). Six scans centered on the optic nerve were obtained. Retinal thickness and morphology were compared between wild-type (WT) rats and *Pde6b* KO rats injected with AAV5-*GFP* or AAV5-*Pde6b.*

Measurement of retinal vessel diameter: We used the Vessel Analysis plugin, which can be added to Fiji to analyze vasculature and allows for the examination and quantitative description of vascular features. The diameters of the retinal vessels were measured at a distance of 1 mm from the optic nerve head in the retina of WT rats and *Pde6b* KO rats injected with AAV5-*GFP* or AAV5-*Pde6b.* The diameters of veins and arteries in one retina were combined to obtain an average value, and the resulting data were converted to micrometers (µm) and displayed on a graph [33].

RNA isolation: RNA was isolated from the retina using the phenol-chloroform extraction method with TRIzol (15,596,026, Thermo Fisher Scientific). Initially, samples were homogenized using a Cordless PELLET PESTLE Motor (749,540-0000, Kimble, Vineland, NJ) with TRIzol. Chloroform was then added to each sample at one-fifth the volume of TRIzol, followed by vortexing for 10 s and centrifugation at 12,000 ×*g* at 4 °C for 15 min. The aqueous phase was then transferred to a new tube, and isopropanol (109634, Merck, Darmstadt, Germany) was added at half the volume of TRIzol. Samples were vortexed briefly for 10 s, followed by centrifugation at 12,000 ×*g* at 4 °C for 15 min. Supernatants were removed and the pellets were washed twice with ice-cold 75% ethanol (E7023, Sigma-Aldrich, St. Louis, MI) prepared in DEPC-treated, nuclease-free water (AM9906, Thermo Fisher Scientific). The pellets were then resuspended in nuclease-free water (AM9937, Thermo Fisher Scientific) and the RNA concentration was determined using a spectrophotometer (Epoch Microplate Spectrophotometer, BioTek, Winooski, VT).

cDNA synthesis: Total RNA (1 µg) was incubated with DNase I (18,068,015, Thermo Fisher Scientific) for 10 min at room temperature, followed by incubation with 25 mM EDTA at 65 °C for 10 min. Subsequently, half of the DNase I-treated RNA was incubated at 70 °C for 5 min to eliminate

the secondary structure within the RNA template. A reverse transcription master mix (EBT-1542, ELPIS-BIOTECH, Dae-jeon, Korea) was then added to the reaction mixture. The mixture was incubated at 37 °C for 30 min, followed by heating at 94 °C for 5 min to synthesize cDNA.

Quantitative reverse transcription PCR: All quantitative PCR (qPCR) primer/probe sets were obtained from IDT (Coralville, IA). cDNA was subjected to real-time qPCR for human PDE6B and rat β-actin, as described in Table 1. PCR was performed using TaqMan Universal Master mix (4324018, Thermo Fisher Scientific) on a real-time PCR system (StepOnePlus, Thermo Fisher Scientific). The PCR reaction began with a 10-min activation at 95 °C, followed by 40 cycles of 95 °C for 15 s (denaturation) and 60 °C for 1 min (annealing and extension). The assays were duplicated for each sample (n=3/group). Normalization was achieved by subtracting the CT values of β-actin from the CT values of human PDE6B using the formula ΔCT = CT value of human PDE6B − CT value of β-actin. mRNA levels of human PDE6B were calculated relative to β-actin using the ΔCT value. For samples where the human PDE6B value was reported as undetermined in the PCR results, the ΔCT value was recorded as 'undetected'.

Retinal pigment epithelial imaging and morphology analysis: The RPE was stained by phalloidin and flat-mounted for retinal pigment cell morphology analysis. The flat-mounted RPE sheet was examined with an LSM 710 fluorescence confocal microscope (Carl Zeiss Microscopy, Jena, Germany). Images of retinal pigment cells were then taken using Zeiss Zen software, black edition (Carl Zeiss Microscopy). RPE images were analyzed by Fiji (Image J; National Institutes of Health, Bethesda, MD) and CellProfiler (Version 4.2.6, Broad Institute, Inc., Cambridge, MA). CellProfiler automatically analyzed retinal pigment epithelial cell size, shape and solidity. Analysis data for the RPE flat mount of each eye was presented as an average value.

Electroretinogram record: Animals were dark-adapted overnight and prepared for recording under dim red illumination. General anesthesia was induced by intraperitoneal administration of a 0.6 mL/kg mixture of tiletamine hypochloride and zolazepam hypochloride (Zoletil; Virbac, Carros, France) and 0.4 ml/kg xylazine hydrochloride (Rompun; Bayer Korea, Seoul, Korea). Topical anesthesia was achieved using proparacaine hydroxychloride (Alcaine; Alcon). After anesthesia was complete, the animal was placed in an earthed aluminum recording chamber and the pupils were fully dilated with eye drops containing 1% tropicamide and 2.5% phenylephrine hydrochloride (Mydrin-P; Santen Pharmaceuticals). A drop of methylcellulose was placed on the corneal surface to ensure electrical contact and to maintain corneal integrity. During ERG recording, rats were placed onto a heating pad to maintain appropriate body temperature. ERGs were recorded from the right eye using the Ganzfeld ERG system (Phoenix Research Laboratories, Bend, OR) with a gold wire loop placed on the right cornea. Reference electrodes were placed in the center of the scalp and ground leads were placed in the skin at the base of the tail. Rod-dominated responses to white light flashes over a 4.0–5.0 log-unit range of intensities were recorded. Signals were sampled every 0.5 ms over a response window of 240 ms. For each stimulus condition, responses were computer-averaged; up to 10 records were averaged for the weakest signals.

Optokinetic nystagmus: To examine visual function for six weeks post-treatment, rats underwent 12 h of dark adaptation, followed by visual stimulation using a digital monitor displaying black-and-white bar patterns 20 cm from the rat's eyes. The monitor was positioned perpendicular to the visual axis. Eye movements were recorded using a digital camera after optodrum video stimulation. Eye movement was quantified by counting the number of times the eyes moved in one direction per minute in the dark room.

Statistics and image analysis: Statistics and ImageJ image analysis software were used to quantify the intensity of the immunofluorescence signals and band densities from immunoblots. Data were analyzed using Statistical Package 429 for the Social Sciences (SPSS) software (version 11.0, IBM, Armonk, NY). Statistical significance was assessed using an ANOVA with Student–Newman–Keuls post hoc analysis.

Table 1. Primer Sequences used for quantitative PCR (qPCR).

Target gene	Direction	Sequence (5'- 3')
Human PDE6B	Forward	CAG TCA GCA GGC TCC TTC
	Reverse	GGT CCT TTA CCA CGT GAA GTG
	Probe	/56-FAM/TG GTT GGC A/ZEN/G GAT GAG CTG GAT/3IABkFQ/
Rat β-actin	Forward	GGA GCC GTT GTC GAC GA
	Reverse	AGT ACA ACC TTC TTG CAG CTC
	Probe	/56-FAM/CC GCC ACC A/ZEN/G TTC GCC ATG/3IABkFQ/

Quantitative data were presented as means ± standard error of the mean (SEM) and differences were considered significant at $p<0.05$.

RESULTS

Noninvasive in vivo green fluorescence protein fluorescence imaging in the retina of Pde6b knockout rats after intravitreal and subretinal injection of AAV2, AAV5 and AAV8 vectors: We compared the efficacy and specificity of three AAV vectors of different serotypes (2, 5 and 8) for delivering genes to the retina of *Pde6b* KO rats in an RP model. We used AAV vectors carrying the green fluorescence protein (GFP) gene under the control of ubiquitous and cytomegalovirus (CMV) promoters and injected them intravitreally or subretinally (Figure 1A,B). The time course of GFP expression was assessed at two, four, and six weeks postinjection and showed the highest level at six weeks (Figure 1E,H,K,N,Q,T). We used in vivo GFP retinal imaging to monitor the transduction and expression of AAV-mediated *GFP* in the retina over time. Within the intravitreal injection group, AAV2-*GFP*-injected *Pde6b* KO rats showed minimal transduction of the inner nuclear layer (Figure 1C,D,E). In contrast, AAV5-*GFP*-injected *Pde6b* KO rats (Figure 1F,G,H) and AAV8-*GFP*-injected *Pde6b* KO rats (Figure 1I,J,K) showed a low number of retinal cells expressing fluorescence. However, within the subretinal injection group, all three serotypes successfully transfected the photoreceptor and RPE, surpassing the effect of the intravitreal AAV2-*GFP* injection, as evidenced by the comparison of fluorescence intensities (Figure 1L-T). Fluorescence increased over time in the subretinal injection group (Figure 1L-T). Interestingly, AAV5-*GFP* had the highest transduction efficiency and the most significant expression area among the serotypes (Figure 1O,P,Q). These results showed that AAV5-*GFP* is an appropriate vector for retinal degeneration gene therapy in *Pde6b* KO rats and that subretinal injection is a better delivery method for achieving the target.

A comparative study of AAV2, AAV5 and AAV8 vectors for retinal gene delivery: evaluating the impact of subretinal and intravitreal injections on efficiency and specificity by immunohistochemistry: To assess the impact of different AAV serotypes (2, 5 and 8) and delivery routes (subretinal and intravitreal injections) on the expression of PDE6B protein in the retina, we performed immunohistochemistry on WT rats (Figure 2A) and *Pde6b* KO rat retinas (Figure 2B). We quantified AAV2-*GFP*, AAV5-*GFP* and AAV8-*GFP* fluorescence intensity in the outer nuclear layer (ONL), inner and outer segments and RPE in the eyes of WT and *Pde6B* KO rats (Figure 2D). Subretinal injection had higher expression than intravitreal injection in WT rats (Figure 2C) and *Pde6b* KO rats (Figure 2D) in the ONL and RPE. These findings demonstrated that AAV5 subretinal injection effectively delivers the *Pde6b* gene to the retina.

AAV5-Pde6b treatment inhibits retinal vessel narrowing in Pde6b knockout rats: Analysis of fundus images reveals significant insights into ocular health [34]. We compared the fundus appearance of WT rats and *Pde6b* KO rats injected with AAV5-*GFP* or AAV5-*Pde6b* (Figure 3C–E). WT rats exhibited standard caliber surface blood vessels indicative of normal vascular structures (Figure 3C). However, *Pde6b* KO rats treated with AAV5-*GFP* exhibited significant irregularities in vascular size (Figure 3D), suggesting underlying pathological alterations [35]. Interestingly, the *Pde6b* KO rats that received AAV5-*Pde6b* showed a mitigated effect on these vascular changes (Figure 3E). Using the Vessel Analysis plugin in Fiji for vasculature analysis has provided significant insights into vascular changes [36]. We found that the increase in complexity of branching patterns in choroidal vessels following AAV5-*GFP*-injected *Pde6b* KO rats compared with WT rats highlighted distinct pathological changes (Figure 3F,G). Conversely, AAV5-*Pde6b* treatment reduced vessel density, suggesting its potential to prevent pathological degeneration (Figure 3H). Furthermore, treatment with AAV5-*Pde6b* resulted in a noticeable increase in the diameter of retinal vessels in *Pde6b* KO rats compared with those treated with AAV5-*GFP* (Figure 3I). These results imply that AAV5-*Pde6b* treatment may prevent the narrowing of vessels in *Pde6b* KO rats, suggesting a potential therapeutic effect of AAV5-*Pde6b* treatment on modulating retinal blood flow.

Restoration of PDE6B protein in Pde6b knockout rats following AAV5-Pde6b treatment: We investigated whether the AAV5-*Pde6b* gene could restore PDE6B expression in a rat model of *Pde6b* deficiency. As shown in Figure 4A, the experimental scheme consisted of subretinal injection of AAV5-*GFP* or AAV5-*Pde6b* in the eyes of *Pde6b* KO rats at postnatal day 21 and analysis of retinal function and morphology at six weeks after injection. RT-PCR analysis showed that increased PDE6B expression in the retinas of AAV5-*Pde6b*-treated KO rats was measured. In contrast, there was no detectable level of PDE6B expression in the retinas of AAV5-GFP-administrated KO rats (Figure 4B). To ascertain the expression of PDE6B protein within the retina's photoreceptor cells, we executed a double immunofluorescence assay, co-staining for PDE6B and Rhodopsin (Figure 4C–H). In WT rats, PDE6B was localized in the photoreceptor outer segment (Figure 4C,F). In *Pde6b* KO rats injected with AAV5-*GFP*, no PDE6B expression was detected

(Figure 4D,G). In contrast, in *Pde6b* KO rats injected with AAV5-*Pde6b*, PDE6B expression was detected in the photoreceptor outer segment (Figure 4E,H). The quantification of PDE6B staining intensity confirmed that AAV5-*Pde6b* treatment significantly increased the expression of PDE6B in the photoreceptor outer segment compared with AAV5-*GFP* administration (Figure 4I). We also found that AAV5-*Pde6b* treatment was able to protect photoreceptors from pathological degeneration in a rat model of *Pde6b* deficiency. The WT rats had regular Rhodopsin expression in the photoreceptor outer segment (Figure 4C,F,J); however, the *Pde6b* KO rats that received AAV5-*GFP* injection had reduced and abnormal

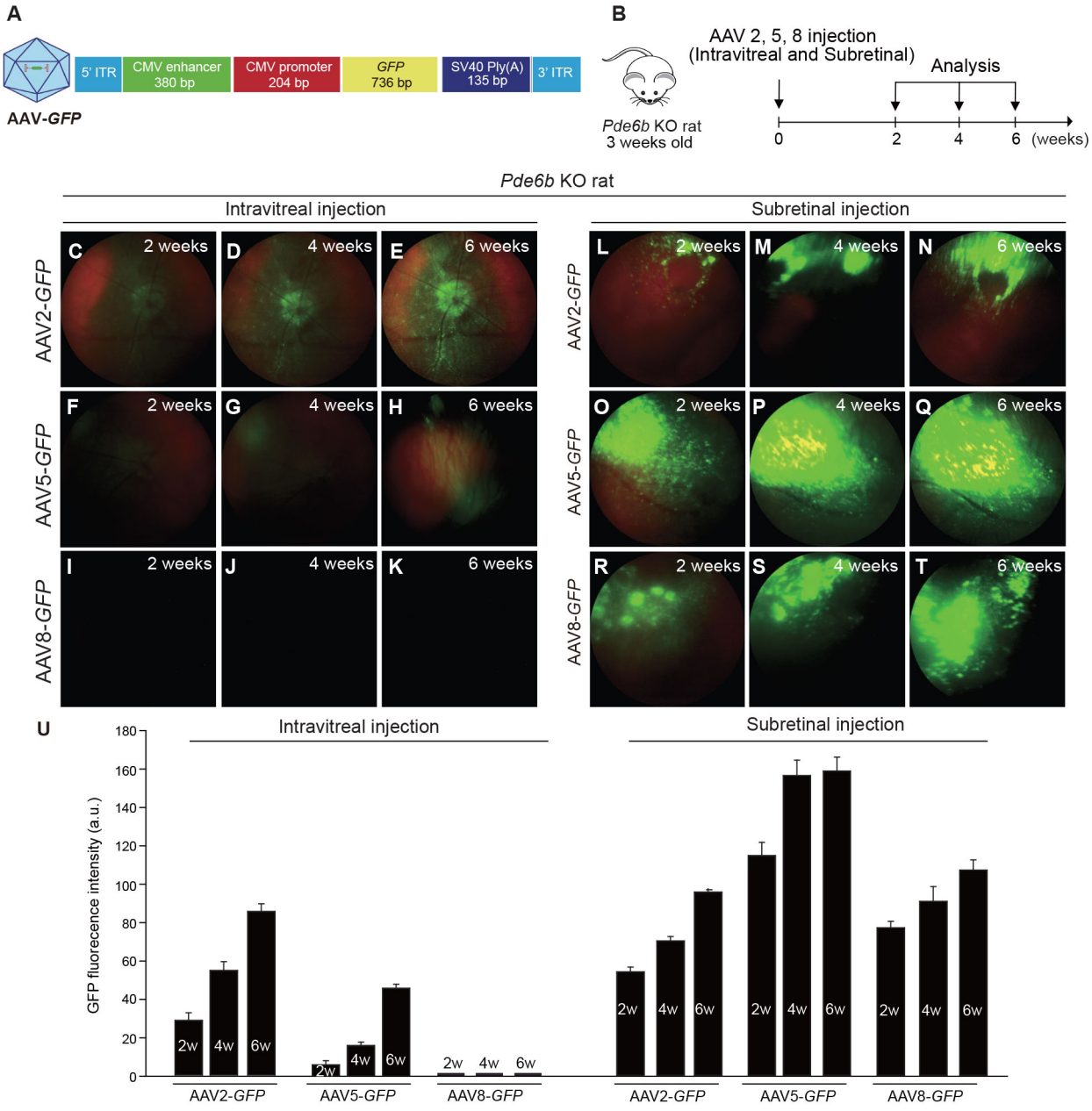

Figure 1. Noninvasive in vivo green fluorescence protein imaging of 2, 5, and 8 adeno-associated virus serotypes based on the delivery route in *Pde6b* knockout rats. **A**: Schematic diagram of the 8 adeno-associated virus (AAV)-*GFP* construct. **B**: Experimental scheme. **C**–**T**: Representative fundus photographs showing green fluorescence protein (GFP) expression in live *Pde6b* knockout rats with intravitreal injection (**C**–**K**) or with subretinal injection (**L**–**T**) of AAV2-*GFP*, AAV5-*GFP* and AAV8-*GFP* vectors at two, four, and six weeks. **U**: Quantification of GFP fluorescence intensity from fundus fluorescent photographs. a.u., arbitrary units. n=4 for each group. Mean fluorescence values were measured over the circular imaging range.

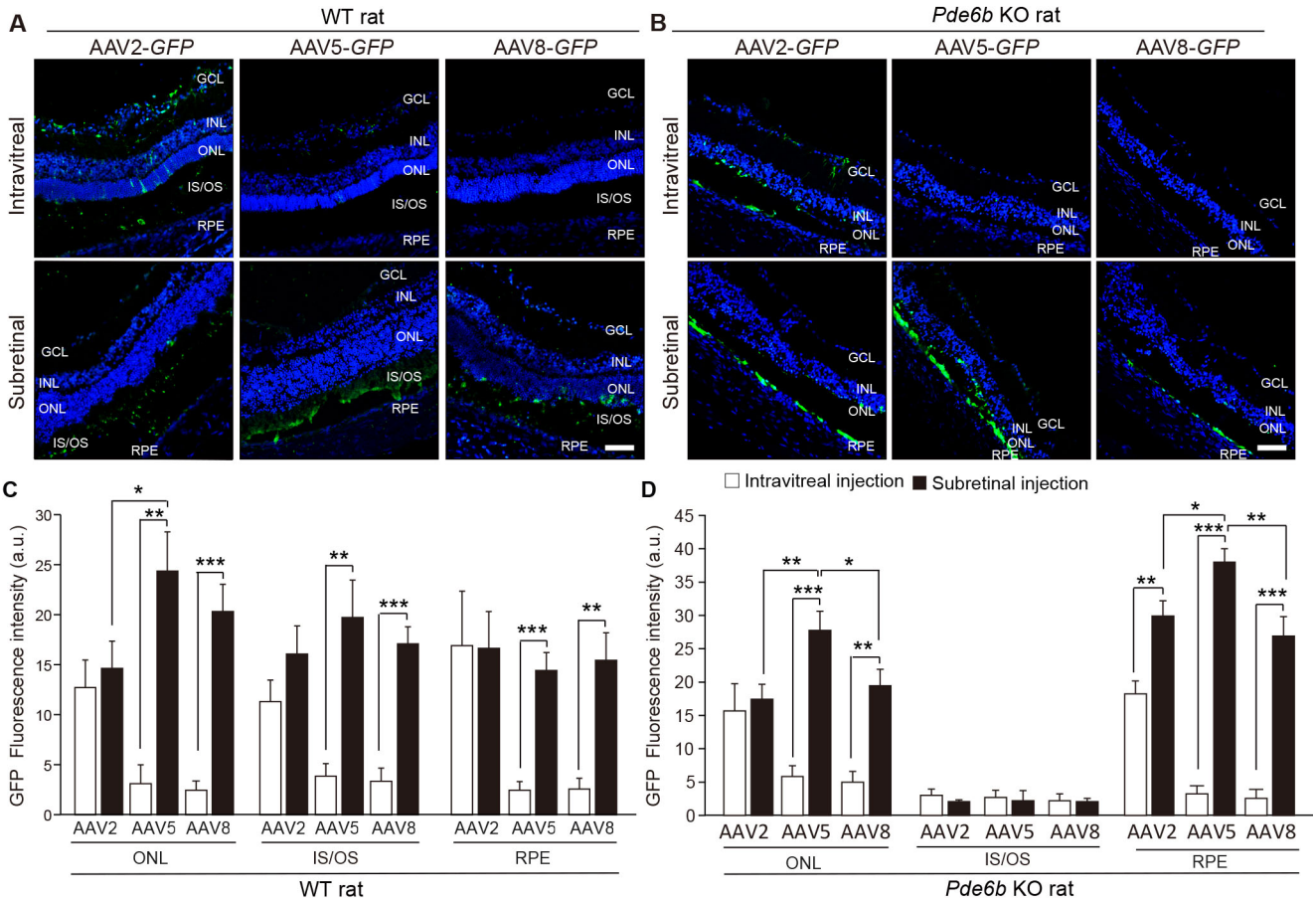

Figure 2. Comparison of green fluorescence protein expression in wild-type and *Pde6b* knockout rat retinas after intravitreal and subretinal injection of different adeno-associated virus vectors. **A**, **B**: Green fluorescence protein (GFP) expression in the retinas of wild-type (WT; **A**) and *Pde6b* knockout (KO) rats (**B**) after intravitreal and subretinal injection of AAV2-*GFP*, AAV5-*GFP* and AAV8-*GFP* vectors at six weeks (n=4 for each group). 4',6-diamidino-2-phenylindole nuclear counterstain is shown in blue. **C**, **D**: Quantitative analysis of AAV2-*GFP*, AAV5-*GFP* and AAV8-*GFP* fluorescence intensity on histological sections in the eyes of WT (C) and *Pde6b* KO rats (D). a.u., arbitrary units; GCL, ganglion cell layer; INL, inner nuclear layer; ONL, outer nuclear layer; IS, inner segments; OS, outer segments; RPE, retinal pigment epithelium. Scale bar, 50 µM. Error bars, mean ± SEM, *p<0.05, **p<0.01, ***p<0.001, ANOVA with Student–Newman–Keuls post hoc analysis.

Rhodopsin expression (Figure 4D,G,J), whereas the *Pde6b* KO rats that received AAV5-*Pde6b* injections had a certain level of Rhodopsin expression in the photoreceptor outer segment (Figure 4E,H,J). The quantification of Rhodopsin immunostaining results showed that AAV5-*Pde6b* treatment maintained Rhodopsin expression in the photoreceptor structure compared with AAV5-*GFP* administration (Figure 4I,J). These results proved that AAV5-*Pde6b* treatment effectively restored PDE6B protein expression and protected photoreceptors from pathological progression in the *Pde6b* KO rats.

AAV5-Pde6b treatment preserves retinal morphology and photoreceptor function in Pde6b knockout rats: We investigated the retinal morphology and photoreceptor function of *Pde6b* KO rats six weeks after receiving AAV5-*Pde6b* injections, as outlined in Figure 5A. Retinal morphology was observed by H&E staining. As indicated in the representative images, there were apparent differences in the thickness of the ONL layer in the AAV5-*GFP*-injected *Pde6b* KO rats compared with that in the WT rats (Figure 5B–D). AAV5-*Pde6b*-injected *Pde6b* KO rats partially preserved the structure of the ONL compared with AAV5-*GFP*-injected *Pde6b* KO rats (Figure 5C,D). Consistent with these findings, the total retinal thickness of the AAV5-*Pde6b*-injected *Pde6b* KO rats was significantly maintained compared with AAV5-*GFP*-injected *Pde6b* KO rats (Figure 5E). Representative OCT images of WT rat retinas and *Pde6b* KO rats injected with AAV5-*GFP* or AAV5-*Pde6b* are shown in Figure 5F–H. OCT images reveal that the cumulative thickness of the ONL,

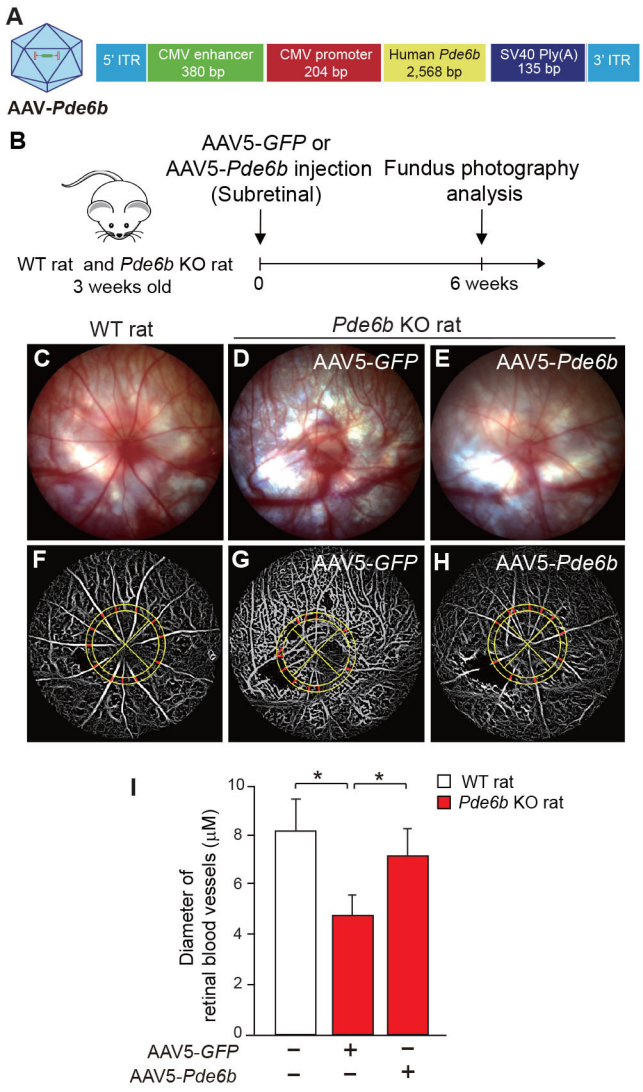

Figure 3. AAV5-*Pde6b* rescues clinical phenotype in *Pde6b* gene knockout rats. **A**: Schematic diagram of the AAV-*Pde6b* construct. **B**: Experimental scheme. **C**–**E**: Representative color fundus photographs of wild-type rats (**C**) and *Pde6b* knockout rats injected with AAV5-*GFP* (**D**) or AAV5-*Pde6b* (**E**; n=4 for each group). **F**–**H**: Total retinal artery and vein analysis in the same rat retina as **C**, **D** and **E**, respectively. Retinal vessel diameters were measured by identifying the vessels marked in red within a yellow circle located at a distance of 1 mm from the optic nerve head in the retina. **I**: Average retinal vessel diameters. Error bars, mean ± SEM, *p<0.05, ANOVA with Student–Newman–Keuls post hoc analysis.

IS layer and OS layer did not appear in the *Pde6b* KO rat compared with WT retinas (Figure 5F,G,I), and this reduction was markedly prevented by AAV5-*Pde6b* injection (Figure 5H,I). Scotopic ERGs were measured to confirm the protective effect of AAV5-*Pde6b* treatment on the degenerative retina of *Pde6b* KO rats. As rod degeneration progressed, A-wave and B-wave amplitudes in AAV5-*GFP*-injected *Pde6b* KO rats dramatically decreased compared with WT rats. However, we found that AAV-*Pde6b* treatment partially restored the A-wave and B-wave amplitudes in *Pde6b* KO rats compared with AAV5-*GFP*-injected *Pde6b* KO rats (Figure 5J,K). We performed optokinetic testing using optokinetic nystagmus as a visual stimulus to assess the visual function of *Pde6b* KO rats administered with AAV5-*Pde6b*. We found that AAV5-*Pde6b*-injected *Pde6b* KO rats showed significant improvement in optokinetic responses at all spatial frequencies tested compared with those of AAV5-*GFP*-injected *Pde6b* KO rats (Figure 5L). These results demonstrate that AAV5-*Pde6b* treatment improved the visual function of *Pde6b* KO rats by protecting the photoreceptor function.

AAV5-Pde6b treatment preserved retinal pigment epithelium barrier function in Pde6b knockout rats: The RPE and photoreceptor cells are closely connected in structure and function [37], and evaluating morphological changes in RPE cells in *Pde6b* KO rats is a critical step in understanding the progression of photoreceptor degeneration. To assess morphological alterations in the RPE cells of *Pde6b* KO rats, we conducted phalloidin immunostaining on RPE whole mounts, investigating the potential therapeutic effect of AAV5-*GFP* and AAV5-*Pde6b* treatment (Figure 6B). In WT rats, RPE cells

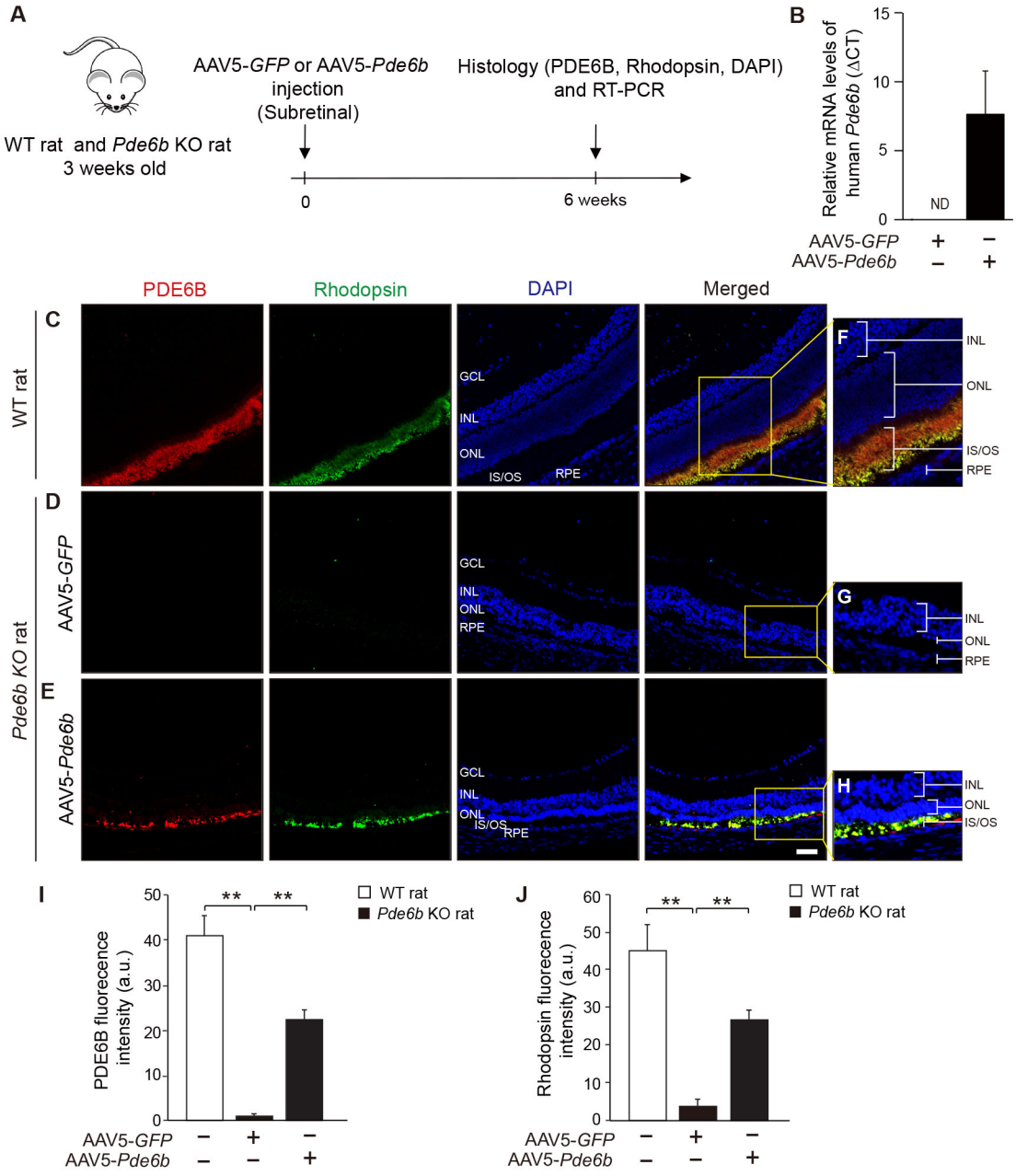

Figure 4. Restoration of PDE6B expression and preservation of photoreceptor cells in *Pde6b* knockout rats following AAV5-*Pde6b* treatment. **A**: Experimental scheme. **B**: Reverse transcriptase PCR analysis of the retinal homogenates from wild-type (WT) and *Pde6b* knockout (KO) rats injected with AAV5-*GFP* or AAV5-*Pde6b* (n=4 for each group). **C**–**E**: Representative images of PDE6B and Rhodopsin in the retina from WT (**C**, **F**) and *Pde6b* KO rats injected with AAV5-*GFP* (D, G) or AAV5-*Pde6b* (**E**, **H**; n=4 for each group). **F**–**H**: Boxed areas on the merged panels are shown at a higher magnification on the left panel. I. Quantification of PDE6B staining intensity in the photoreceptor outer segment. **J**: Quantification of Rhodopsin staining intensity in the photoreceptor outer segment. 4',6-diamidino-2-phenylindole nuclear counterstain is shown in blue. a.u., arbitrary units; GCL, ganglion cell layer; INL, inner nuclear layer; ONL, outer nuclear layer; IS/OS, inner and outer segments; RPE, retinal pigment epithelium. Scale bar, 50 µM. Error bars, mean ± SEM, **p<0.01, ANOVA with Student–Newman–Keuls post hoc analysis.

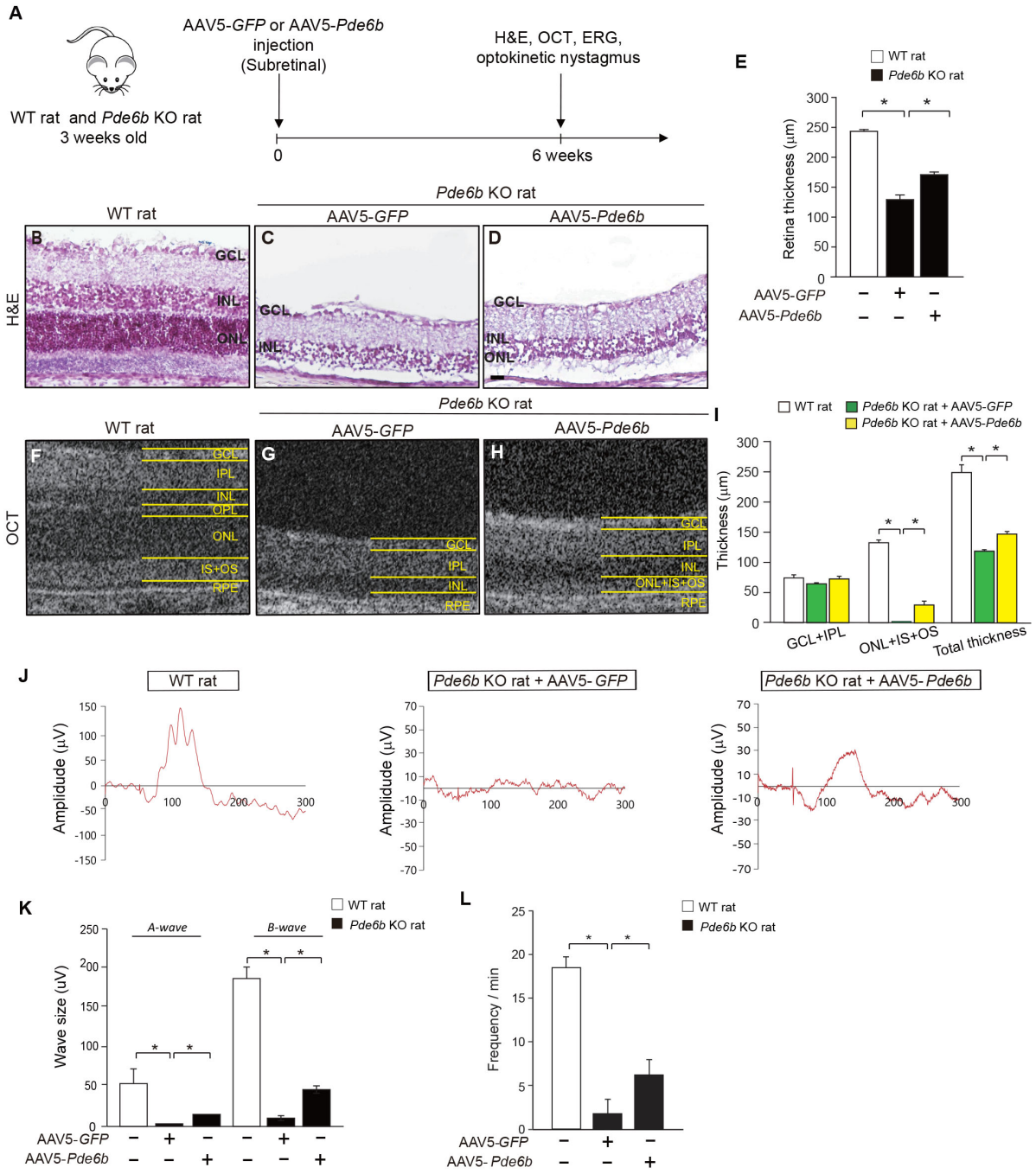

Figure 5. AAV5-*Pde6b* treatment protected retinal cell layers and improved visual function in *Pde6b* knockout rats. **A**: Experimental scheme. **B**–**D**: Representative images of hematoxylin and eosin staining in the retina of wild-type (WT) rats (**B**) and *Pde6b* knockout (KO) rats injected with AAV5-*GFP* (**C**) or AAV5-*Pde6b* (D; n=4 for each group). E. Quantification of the retinal thicknesses. **F**–**H**: Representative images of in vivo optical coherence tomography scans of WT rats (**F**) and *Pde6b* KO rats injected with AAV5-*GFP* (G) or AAV5-*Pde6b* (**H**; n=4 for each group). **I**: Quantification of the thickness of the separated layer. **J**: Representative electroretinogram responses to light stimulus. K. Quantitative analysis of the scotopic A-wave and B-wave (n=4 for each group). **L**: Quantitative eye movement analysis by optokinetic nystagmus test (n=4 for each group). GCL, ganglion cell layer; IPL, inner plexiform; INL, inner nuclear layer; OPL, outer plexiform layer; ONL, outer nuclear layer; IS, inner segments; OS, outer segments; RPE, retinal pigment epithelium. Scale bar, 50 μM. Error bars, mean ± SEM, *p<0.01, ANOVA with Student–Newman–Keuls post hoc analysis.

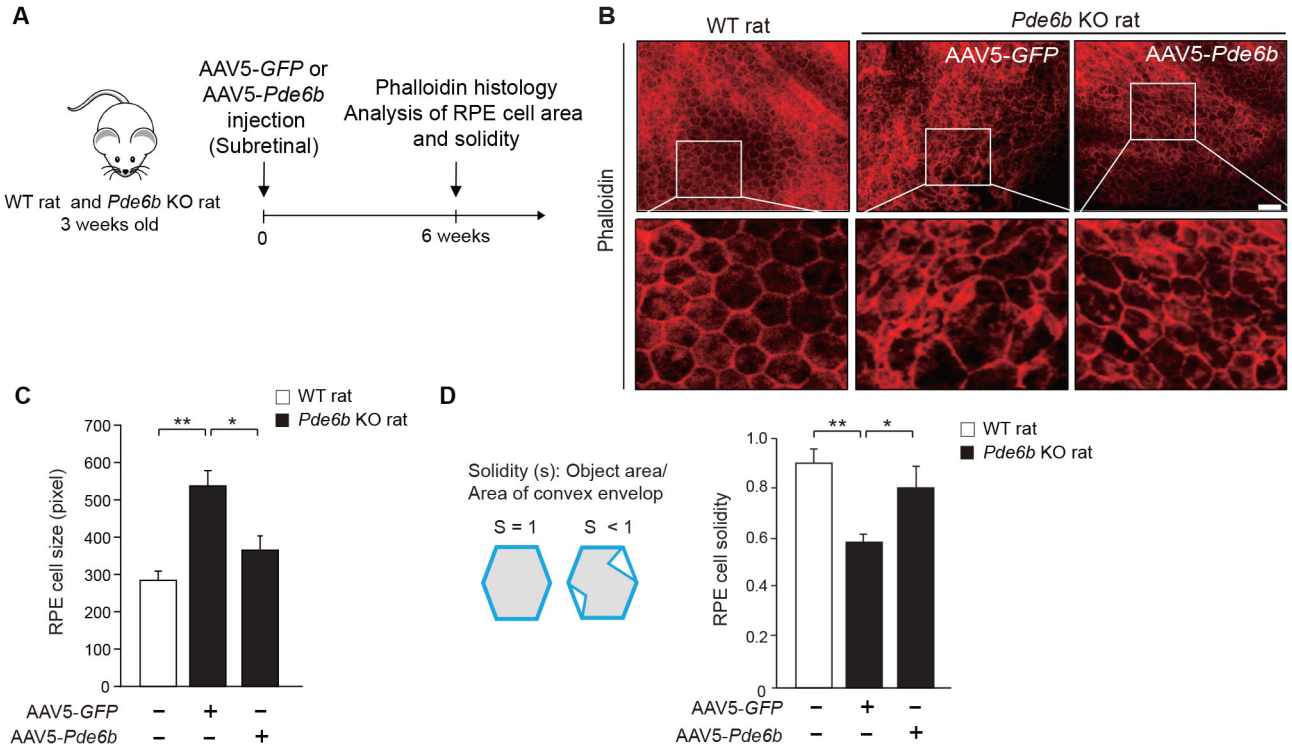

Figure 6. AAV5-*Pde6b* treatment preserved retinal pigment epithelial barrier function in *Pde6b* knockout rats. **A**: Experimental scheme. **B**: Representative image of Phalloidin-stained retinal pigment epithelium (RPE) cells (n=4 for each group). Boxed areas on the top panels were shown at a higher magnification on the bottom panel. Scale bar, 50 µM. **C**, **D**: Quantification of individual RPE cell parameters: RPE cell size (**C**) and RPE cell solidity (**D**). Error bars, mean ± SEM, *p<0.05, **p<0.01, ANOVA with Student–Newman–Keuls post hoc analysis.

typically exhibit a consistent size (Figure 6C). In contrast, *Pde6b* KO rats that received AAV5-*GFP* treatment demonstrated RPE cells of various sizes, as depicted in Figure 6C. The administration of AAV5-*Pde6b* in *Pde6b* KO rats led to a normalization of RPE cell size (Figure 6C). We also analyzed cell solidity (the proportion of the RPE cell area filling a best-fit convex envelope). Our findings revealed that the RPE cells of *Pde6b* KO rats injected with AAV5-*GFP* exhibited a marked decrease in solidity compared with WT rats. Conversely, *Pde6b* KO rats treated with AAV5-*Pde6b* showed increased cell solidity compared with AAV5-*GFP*-injected rats (Figure 6D).

DISCUSSION

In this study, we present the promising potential of AAV5-*Pde6b* under the CMV promoter as a therapeutic gene candidate for treating RP caused by *Pde6b* deficiency. Our findings demonstrate that AAV5-*Pde6b* vectors effectively improve photoreceptor response to light as well as the visual function of RP rats. The preservation of both A-wave and B-wave in the scotopic ERG responses, which mirrors the rescue effect observed in H&E staining and fundus imaging, is a significant step forward in the development of gene therapy for RP.

Gene therapy is a promising approach for treating various ocular diseases, such as inherited retinal dystrophies, age-related macular degeneration, glaucoma and corneal disorders [38,39]. Among various gene delivery vectors used for gene therapy, AAVs are the most widely adopted due to their beneficial features of safety, stability and efficiency [5]. Different AAV serotypes have shown different transduction profiles of their specific cell and tissue targets [18,40]. Thus, the optimal AAV serotype and injection route for treating patients with different retinal diseases may maximize the therapeutic effect.

Coave Therapeutics, the French clinical stage biotechnology company, has been developing several gene therapeutic candidates for rare ocular and central nervous system diseases (COAVETX). Although Coave Therapeutics announced positive data from their ongoing Phase I/II clinical trial on CTx-PDE6b (AAV5-*Pde6b* vectors under the Rhodopsin kinase promoter) in patients with RP on May 31, 2023 (COAVETX), we designed the several novel AAV5-*Pde6b* vectors under the CMV promoter as well as other

ocular tissue-specific promoters to develop more efficient therapeutic gene vectors for treating RP patients with *Pde6b* mutations. Here, we summarized the potential therapeutic effects of AAV5-*Pde6b* under the CMV promoter when AAV5-*Pde6b* was injected in *Pde6b* KO rats. We demonstrated the therapeutic efficacy of protecting retinal cell layers, including photoreceptors and the RPE monolayer and improving visual function, as confirmed by scotopic ERG responses and optokinetic eye movements in *Pde6b* KO rats administered with AAV5-*Pde6b.*

The RPE is a single-cell layer between the retina's photoreceptor outer segments (POS) and Bruch's membrane, and RPE cells maintain retinal health and function [37]. Some of their essential functions include forming the outer blood-retinal barrier (BRB), delivering oxygen and nutrients from the choroid to the outer retina, clearing metabolic waste from the outer retina to the choroid, and regulating the immune response in the subretinal space [41-43]. In RP, the RPE morphology is altered by photoreceptor degeneration and lipofuscin, a waste product of phototransduction, buildup [44,45]. The RPE cells become uneven in shape and size, and show changes in pigmentation [46,47]. These changes can be detected by fundus examination or histological staining of RPE markers such as phalloidin. Our investigation demonstrated that AAV5-*Pde6b* treatment of *Pde6b* KO rats suppressed degenerative progression in photoreceptors. In addition, it was confirmed that by preserving the photoreceptor, progressive degeneration of RPE cells adjacent to the photoreceptor, which may lead to secondary impairment, was partially prevented.

In this study, we conducted a short-term efficacy trial (six weeks) to investigate the expression and efficacy of AAV5-CMV-*Pde6b* in *Pde6b* KO mice. We are currently working to optimize the AAV5-*Pde6b* vector with cell-specific promoters and vary dosages to improve precision of the treatment. If a lead compound is identified, we will conduct long-term efficacy trials at six and 12 months. This will provide valuable insight into the durability of therapeutic benefits and potential delayed side effects. This rigorous approach will confirm our initial findings and enrich the scientific community's understanding of the long-term impact of gene therapy in retinal diseases, ultimately paving the way for clinical applications. The variability in gene therapy's long-term effects and side effects, contingent upon the method of administration, necessitates vigilant monitoring and assessment during clinical trials. An initial gene therapy injection may show promising results, but its efficacy could wane. Our use of a singular dose of the AAV5-*Pde6b* vector in treating *Pde6b*-deficient rats may not represent the optimal approach for the most favorable therapeutic outcome. The literature indicates that varying AAV vector dosages can significantly influence transgene expression and immune reactions, as well as the safety profile [48,49]. Thus, the application and dosage of gene therapy will likely vary based on the type of disease, the extent and progression of retinal degeneration and patient-specific factors such as age, weight and overall health [50,51].

In light of these considerations, future research should delve into the dose–response relationship of our gene therapy to pinpoint the optimal dosage that maximizes efficacy while minimizing toxicity. Such investigations will be pivotal in fine-tuning gene therapy protocols for retinal diseases, ensuring safety and effectiveness in long-term therapeutic applications. In conclusion, our findings suggest that AAV5-mediated subretinal *Pde6b* gene delivery strongly supports the therapeutic potential of AAV5-*Pde6b* gene therapy as a promising gene therapy approach for RP caused by *Pde6b* mutations. The observed results highlight the ability to address the underlying genetic causes and prevent the degenerative progression associated with RP symptoms. Following this study and ongoing investigation, nonclinical studies and early phases of clinical studies may verify its therapeutic efficacy, long-term safety, potential application and clinical applicability as a valuable therapeutic intervention for treating RP patients.

ACKNOWLEDGMENTS

Author Contributions: H.J.K., J.H.K., J.K., S.Y.M., and. J.S.C. performed the in vivo experiments and analyzed the data; J.S.C. and J.Y.L. planned and analyzed the mouse models. S.H.S.L., K.P., H.L., and J.Y.L. reviewed and edited the manuscript. J.S.C., K.P., and J.Y.L. provided technical advice about the experimental design; S.Y.W. designed and analyzed the data and wrote the paper. All authors have read and agreed to the published version of the manuscript. Funding: This research was supported by the Korea Drug Development Fund, funded by the Ministry of Science and ICT, the Ministry of Trade, Industry, and Energy, and the Ministry of Health and Welfare (HN22C0245, Republic of Korea). Declarations: Ethics approval and consent to participate No consent to participate was required for this study. Consent for publication: All authors consented to publication. Conflicts of Interest: H.J.K., J.S.C., J.K., S.Y.M., S.H.S.L., K.P., and S.Y.W. are employees of CdmoGen Co., Ltd., in which S.H.S.L. and K.P. have personal financial interests. No other potential conflicts of interest relevant to this article were reported. Dr. Joo Yong Lee (jylee.retina@gmail.com) and Dr. So-Yoon Won (sywon@cdmogen.com) are co-corresponding authors for this paper.

REFERENCES

1. Kamde SP, Anjankar A. Retinitis Pigmentosa: Pathogenesis, Diagnostic Findings, and Treatment. Cureus 2023; 15:e48006[PMID: 38034182].
2. Hartong DT, Berson EL, Dryja TP. Retinitis pigmentosa. Lancet 2006; 368:1795-809. [PMID: 17113430].
3. Bhattacharya S, Lester D, Keen J, Bashir R, Lauffart B, Inglehearn CF, Jay M, Bird AC. Retinitis pigmentosa and mutations in rhodopsin. Lancet 1991; 337:185-[PMID: 1670831].
4. O'Neal TB, Luther EE. Retinitis Pigmentosa. StatPearls. Publishing. 2023.
5. Naso MF, Tomkowicz B, Perry WL 3rd, Strohl WR. Adeno-Associated Virus (AAV) as a Vector for Gene Therapy. BioDrugs 2017; 31:317-34. [PMID: 28669112].
6. Tsang SH, Sharma T. Retinitis Pigmentosa (Non-syndromic). Adv Exp Med Biol 2018; 1085:125-30. [PMID: 30578498].
7. Kim YN, Song JS, Oh SH, Kim YJ, Yoon YH, Seo EJ, Seol CA, Lee SM, Choi JM, Seo GH, Keum C, Lee BH, Lee JY. Clinical characteristics and disease progression of retinitis pigmentosa associated with PDE6B mutations in Korean patients. Sci Rep 2020; 10:19540-[PMID: 33177553].
8. Cote RH, Gupta R, Irwin MJ, Wang X. Photoreceptor Phosphodiesterase (PDE6): Structure, Regulatory Mechanisms, and Implications for Treatment of Retinal Diseases. Adv Exp Med Biol 2022; 1371:33-59. [PMID: 34170501].
9. Cote RH. Photoreceptor phosphodiesterase (PDE6): activation and inactivation mechanisms during visual transduction in rods and cones. Pflugers Arch 2021; 473:1377-91. [PMID: 33860373].
10. Li S, Ma H, Yang F, Ding X. cGMP Signaling in Photoreceptor Degeneration. Int J Mol Sci 2023; 24:24-[PMID: 37446378].
11. Oishi M, Oishi A, Gotoh N, Ogino K, Higasa K, Iida K, Makiyama Y, Morooka S, Matsuda F, Yoshimura N. Comprehensive molecular diagnosis of a large cohort of Japanese retinitis pigmentosa and Usher syndrome patients by next-generation sequencing. Invest Ophthalmol Vis Sci 2014; 55:7369-75. [PMID: 25324289].
12. Kim MS, Joo K, Seong MW, Kim MJ, Park KH, Park SS, Woo SJ. Genetic Mutation Profiles in Korean Patients with Inherited Retinal Diseases. J Korean Med Sci 2019; 34:e161[PMID: 31144483].
13. Kang C, Scott LJ. Voretigene Neparvovec: A Review in RPE65 Mutation-Associated Inherited Retinal Dystrophy. Mol Diagn Ther 2020; 24:487-95. [PMID: 32535767].
14. Cano M, Datta S, Wang L, Liu T, Flores-Bellver M, Sachdeva M, Sinha D, Handa JT. Nrf2 deficiency decreases NADPH from impaired IDH shuttle and pentose phosphate pathway in retinal pigmented epithelial cells to magnify oxidative stress-induced mitochondrial dysfunction. Aging Cell 2021; 20:e13444[PMID: 34313391].
15. Wu DM, Ji X, Ivanchenko MV, Chung M, Piper M, Rana P, Wang SK, Xue Y, West E, Zhao SR, Xu H, Cicconet M, Xiong W, Cepko CL. Nrf2 overexpression rescues the RPE in mouse models of retinitis pigmentosa. JCI Insight 2021; 6:6-[PMID: 33491671].
16. Drag S, Dotiwala F, Upadhyay AK. Gene Therapy for Retinal Degenerative Diseases: Progress, Challenges, and Future Directions. Invest Ophthalmol Vis Sci 2023; 64:39-[PMID: 37389545].
17. Lee JH, Wang JH, Chen J, Li F, Edwards TL, Hewitt AW, Liu GS. Gene therapy for visual loss: Opportunities and concerns. Prog Retin Eye Res 2019; 68:31-53. [PMID: 30170104].
18. Zincarelli C, Soltys S, Rengo G, Rabinowitz JE. Analysis of AAV serotypes 1-9 mediated gene expression and tropism in mice after systemic injection. Mol Ther 2008; 16:1073-80. [PMID: 18414476].
19. Han IC, Cheng JL, Burnight ER, Ralston CL, Fick JL, Thomsen GJ, Tovar EF, Russell SR, Sohn EH, Mullins RF, Stone EM, Tucker BA, Wiley LA. Retinal Tropism and Transduction of Adeno-Associated Virus Varies by Serotype and Route of Delivery (Intravitreal, Subretinal, or Suprachoroidal) in Rats. Hum Gene Ther 2020; 31:1288-99. [PMID: 32948113].
20. Sun YJ, Lin CH, Wu MR, Lee SH, Yang J, Kunchur CR, Mujica EM, Chiang B, Jung YS, Wang S, Mahajan VB. An intravitreal implant injection method for sustained drug delivery into mouse eyes. Cell Rep Methods 2021; 1:1-[PMID: 35128514].
21. Irigoyen C, Amenabar Alonso A, Sanchez-Molina J, Rodríguez-Hidalgo M, Lara-López A, Ruiz-Ederra J. Subretinal Injection Techniques for Retinal Disease: A Review. J Clin Med 2022; 11:11-[PMID: 36012955].
22. Tranos P, Tsiropoulos GN, Koronis S, Vakalis A, Asteriadis S, Stavrakas P. Comparison of subretinal versus intravitreal injection of recombinant tissue plasminogen activator with gas for submacular hemorrhage secondary to wet age-related macular degeneration: treatment outcomes and brief literature review. Int Ophthalmol 2021; 41:4037-46. [PMID: 34331185].
23. Davis RJ, Tosi J, Janisch KM, Kasanuki JM, Wang NK, Kong J, Tsui I, Cilluffo M, Woodruff ML, Fain GL, Lin CS, Tsang SH. Functional rescue of degenerating photoreceptors in mice homozygous for a hypomorphic cGMP phosphodiesterase 6 b allele (Pde6bH620Q). Invest Ophthalmol Vis Sci 2008; 49:5067-76. [PMID: 18658088].
24. Allocca M, Manfredi A, Iodice C, Di Vicino U, Auricchio A. AAV-mediated gene replacement, either alone or in combination with physical and pharmacological agents, results in partial and transient protection from photoreceptor degeneration associated with betaPDE deficiency. Invest Ophthalmol Vis Sci 2011; 52:5713-9. [PMID: 21273543].
25. Aitman T, Dhillon P, Geurts AM. A RATional choice for translational research? Dis Model Mech 2016; 9:1069-72. [PMID: 27736742].
26. Smalley E. CRISPR mouse model boom, rat model renaissance. Nat Biotechnol 2016; 34:893-4. [PMID: 27606442].
27. Shirai H, Mandai M, Matsushita K, Kuwahara A, Yonemura S, Nakano T, Assawachananont J, Kimura T, Saito K, Terasaki H, Eiraku M, Sasai Y, Takahashi M. Transplantation

of human embryonic stem cell-derived retinal tissue in two primate models of retinal degeneration. Proc Natl Acad Sci U S A 2016; 113:E81-90. [PMID: 26699487].

28. Zhu L, Jang GF, Jastrzebska B, Filipek S, Pearce-Kelling SE, Aguirre GD, Stenkamp RE, Acland GM, Palczewski K. A naturally occurring mutation of the opsin gene (T4R) in dogs affects glycosylation and stability of the G protein-coupled receptor. J Biol Chem 2004; 279:53828-39. [PMID: 15459196].

29. Rah H, Maggs DJ, Blankenship TN, Narfstrom K, Lyons LA. Early-onset, autosomal recessive, progressive retinal atrophy in Persian cats. Invest Ophthalmol Vis Sci 2005; 46:1742-7. [PMID: 15851577].

30. Li SY, Yin ZQ, Chen SJ, Chen LF, Liu Y. Rescue from light-induced retinal degeneration by human fetal retinal transplantation in minipigs. Curr Eye Res 2009; 34:523-35. [PMID: 19899965].

31. Nishida K, Kamei M, Kondo M, Sakaguchi H, Suzuki M, Fujikado T, Tano Y. Efficacy of suprachoroidal-transretinal stimulation in a rabbit model of retinal degeneration. Invest Ophthalmol Vis Sci 2010; 51:2263-8. [PMID: 19933186].

32. Yeo JH, Jung BK, Lee H, Baek IJ, Sung YH, Shin HS, Kim HK, Seo KY, Lee JY. Development of a Pde6b Gene Knockout Rat Model for Studies of Degenerative Retinal Diseases. Invest Ophthalmol Vis Sci 2019; 60:1519-26. [PMID: 31009522].

33. Zarb Y, Weber-Stadlbauer U, Kirschenbaum D, Kindler DR, Richetto J, Keller D, Rademakers R, Dickson DW, Pasch A, Byzova T, Nahar K, Voigt FF, Helmchen F, Boss A, Aguzzi A, Klohs J, Keller A. Ossified blood vessels in primary familial brain calcification elicit a neurotoxic astrocyte response. Brain 2019; 142:885-902. [PMID: 30805583].

34. Cen LP, Ji J, Lin JW, Ju ST, Lin HJ, Li TP, Wang Y, Yang JF, Liu YF, Tan S, Tan L, Li D, Wang Y, Zheng D, Xiong Y, Wu H, Jiang J, Wu Z, Huang D, Shi T, Chen B, Yang J, Zhang X, Luo L, Huang C, Zhang G, Huang Y, Ng TK, Chen H, Chen W, Pang CP, Zhang M. Automatic detection of 39 fundus diseases and conditions in retinal photographs using deep neural networks. Nat Commun 2021; 12:4828-[PMID: 34376678].

35. Hamel C. Retinitis pigmentosa. Orphanet J Rare Dis 2006; 1:40-[PMID: 17032466].

36. Callewaert B, Gsell W, Himmelreich U, Jones EAV. Q-VAT: Quantitative Vascular Analysis Tool. Front Cardiovasc Med 2023; 10:1147462[PMID: 37332588].

37. Yang S, Zhou J, Li D. Functions and Diseases of the Retinal Pigment Epithelium. Front Pharmacol 2021; 12:727870[PMID: 34393803].

38. Ameri H, Kesavamoorthy N, Bruce DN. Frequency and Pattern of Worldwide Ocular Gene Therapy Clinical Trials up to 2022. Biomedicines 2023; 11:11-[PMID: 38137345].

39. Lee SH, Kim YS, Nah SK, Kim HJ, Park HY, Yang JY, Park K, Park TK. Transduction Patterns of Adeno-associated Viral Vectors in a Laser-Induced Choroidal Neovascularization Mouse Model. Mol Ther Methods Clin Dev 2018; 9:90-8. [PMID: 29766021].

40. Westhaus A, Eamegdool SS, Fernando M, Fuller-Carter P, Brunet AA, Miller AL, Rashwan R, Knight M, Daniszewski M, Lidgerwood GE, Pébay A, Hewitt A, Santilli G, Thrasher AJ, Carvalho LS, Gonzalez-Cordero A, Jamieson RV, Lisowski L. AAV capsid bioengineering in primary human retina models. Sci Rep 2023; 13:21946-[PMID: 38081924].

41. Bhutto I, Lutty G. Understanding age-related macular degeneration (AMD): relationships between the photoreceptor/retinal pigment epithelium/Bruch's membrane/choriocapillaris complex. Mol Aspects Med 2012; 33:295-317. [PMID: 22542780].

42. O'Leary F, Campbell M. The blood-retina barrier in health and disease. FEBS J 2023; 290:878-91. [PMID: 34923749].

43. Braunger BM, Gießl A, Schlötzer-Schrehardt U. The Blood-ocular Barriers and their Dysfunction: Anatomy, Physiology, Pathology. Klin Monbl Augenheilkd 2023; 240:650-61. [PMID: 37207638].

44. Kim YK, Yu H, Summers VR, Donaldson KJ, Ferdous S, Shelton D, Zhang N, Chrenek MA, Jiang Y, Grossniklaus HE, Boatright JH, Kong J, Nickerson JM. Morphometric Analysis of Retinal Pigment Epithelial Cells From C57BL/6J Mice During Aging. Invest Ophthalmol Vis Sci 2021; 62:32-[PMID: 33616620].

45. Adler L 4th, Chen C, Koutalos Y. All-trans retinal levels and formation of lipofuscin precursors after bleaching in rod photoreceptors from wild type and Abca4$^{-/-}$ mice. Exp Eye Res 2017; 155:121-7. [PMID: 28219732].

46. Ortolan D, Sharma R, Volkov A, Maminishkis A, Hotaling NA, Huryn LA, Cukras C, Di Marco S, Bisti S, Bharti K. Single-cell-resolution map of human retinal pigment epithelium helps discover subpopulations with differential disease sensitivity. Proc Natl Acad Sci U S A 2022; 119:e2117553119[PMID: 35522714].

47. Costa BLD, Quinn PMJ, Wu WH, Liu S, Nolan ND, Demirkol A, Tsai YT, Caruso SM, Cabral T, Wang NK, Tsang SH. Targeting miR-181a/b in retinitis pigmentosa: implications for disease progression and therapy. Cell Biosci 2024; 14:64-[PMID: 38773556].

48. Khabou H, Cordeau C, Pacot L, Fisson S, Dalkara D. Dosage Thresholds and Influence of Transgene Cassette in Adeno-Associated Virus-Related Toxicity. Hum Gene Ther 2018; 29:1235-41. [PMID: 30132368].

49. Costa Verdera H, Kuranda K, Mingozzi F. AAV Vector Immunogenicity in Humans: A Long Journey to Successful Gene Transfer. Mol Ther 2020; 28:723-46. [PMID: 31972133].

50. Vandenberghe LH, Bell P, Maguire AM, Cearley CN, Xiao R, Calcedo R, Wang L, Castle MJ, Maguire AC, Grant R, Wolfe JH, Wilson JM, Bennett J. Dosage thresholds for AAV2 and AAV8 photoreceptor gene therapy in monkey. Sci Transl Med 2011; 3:88ra54[PMID: 21697530].

51. Ay C, Reinisch A. Gene therapy: principles, challenges and use in clinical practice. Wien Klin Wochenschr 2024; [PMID: 38713227].